THE JOURNAL OF BIOLOGICAL CHEMISTRY VOL. 292, NO. 11, pp. 4411–4422, March 17, 2017

Small GTPase Rab8a-recruited Phosphatidylinositol 3-Kinase γ Regulates Signaling and Cytokine Outputs from Endosomal Toll-like Receptors*[S]

Received for publication, November 3, 2016, and in revised form, January 14, 2017 Published, JBC Papers in Press, January 27, 2017, DOI 10.1074/jbc.M116.766337

Adam A. Wall[‡1], **Lin Luo**[‡1], **Yu Hung**[‡], **Samuel J. Tong**[‡], **Nicholas D. Condon**[‡], **Antje Blumenthal**[§], **Matthew J. Sweet**[‡], **and Jennifer L. Stow**[‡2]

From the [‡]*Institute for Molecular Bioscience (IMB) and IMB Centre for Inflammation and Disease Research, University of Queensland, Brisbane, Queensland 4072, Australia and the* [§]*University of Queensland Diamantina Institute, University of Queensland, Translational Research Institute, Brisbane, Queensland 4102, Australia*

Edited by Luke O'Neill

LPS-mediated activation of Toll-like receptor 4 (TLR4) in macrophages results in the coordinated release of proinflammatory cytokines, followed by regulatory mediators, to ensure that this potentially destructive pathway is tightly regulated. We showed previously that Rab8a recruits PI3Kγ for Akt-dependent signaling during TLR4 activation to limit the production of the proinflammatory cytokines IL-6 and IL-12p40 while enhancing the release of the regulatory/anti-inflammatory cytokine IL-10. Here we broaden the array of immune receptors controlled by Rab8a-PI3Kγ and further define the Rab-mediated membrane domains required for signaling. With CRISPR/Cas9-mediated gene editing to stably knock out and recover Rab8a in macrophage cell lines, we match Akt signaling profiles with cytokine outputs, confirming that Rab8a is a novel regulator of the Akt/mammalian target of rapamycin (mTOR) pathway downstream of multiple TLRs. Upon developing a Rab8a activation assay, we show that TLR3 and 9 agonists also activate Rab8a. Live-cell imaging reveals that Rab8a is first recruited to the plasma membrane and dorsal ruffles, but it is retained during collapse of ruffles to form macropinosomes enriched for phosphatidylinositol 3,4,5-trisphosphate ($PI(3,4,5)P_3$) and phosphatidylinositol 3,4-bisphosphate ($PI(3,4)P_2$), suggesting that the macropinosome is the location where Rab8a is active. We pinpoint macropinosomes as the sites for Rab8-mediated biasing of inflammatory signaling responses via inducible production of anti-inflammatory cytokines. Thus, Rab8a and PI3Kγ are positioned in multiple TLR pathways, and this signaling axis may serve as a pharmacologically tractable target during infection and inflammation.

Toll-like receptors (TLRs),[3] a key family of pattern recognition receptors, activate macrophages upon detection of pathogens and/or danger signals (1). Members of this family respond to molecular signatures of different pathogens, and the ensuing signaling and transcriptional responses are required to mount frontline innate immune defenses to help fight infection. These responses include the expression and secretion of inflammatory and regulatory cytokines and chemokines (2). Several mechanisms serve to tailor the signaling output of TLR pathways toward immune responses against different types of pathogens. The Toll/interleukin-1 receptor (TIR) domain-containing adaptors at the plasma membrane as well as in endosomes or phagosomes provide spatiotemporal control of TLR signaling (3). For example, myeloid differentiation primary response gene 88 (MyD88) and MyD88-adapter-like (Mal) couple with TLR4 at the cell surface, whereas TRIF and TRAM generate signaling from endosomal compartments in response to LPS (4). Other TLR family members have thus far been shown to only signal from either the cell surface or from endosomal compartments. Viral and host double-stranded RNAs activate TLR3 (with TRIF) (5), whereas endosomal non-methylated CpG DNA motifs activate TLR9 (with MyD88) to signal from endosomal compartments (6). The membrane domains and signaling environments at the cell surface and in endosomal compartments are defined and differentiated by the adaptors and by factors such as membrane phosphoinositides (7). These factors vary signaling and cytokine outputs that drive and define the regulatory or anti-inflammatory states that help to curtail inflammation and avoid disease (8).

Class 1A PI3Ks contribute to signaling downstream of TLRs. We revealed previously that the class1B PI3Kγ regulates Akt/mTOR signaling downstream of LPS-activated TLR4 (9). Unusually, the GTPase Rab8a recruits the PI3Kγ catalytic subunit (p110γ) to membranes for this role in TLR4 signaling. Activation of Rab8a and PI3Kγ constrains the secretion of the proinflammatory cytokines IL-6 and IL-12p40 while enhancing

* This work was supported by the National Health and Medical Research Council of Australia (Fellowship APP1003021 to J. L. S., Grant APP1098710 to J. L. S. and A. B., and Senior Research Fellowship APP1107914 to M. J. S.) and was supported by the Australian Infectious Diseases Research Centre. The authors declare that they have no conflicts of interest with the contents of this article.
[S] This article contains supplemental Figs. S1–S5.
[1] Both authors contributed equally to this work.
[2] To whom correspondence should be addressed: E-mail: j.stow@imb.uq.edu.au.
[3] The abbreviations used are: TLR, Toll-like receptor; mTOR, mammalian target of rapamycin; WGA, wheat germ agglutinin; Tfn, transferrin; PH, pleckstrin homology; CREB, cAMP-response element-binding protein; HMDM, human monocyte-derived macrophage; RBD, Ras-binding domain; BMM, bone marrow-derived macrophage; CSF, colony-stimulating factor; ANOVA, analysis of variance; PI(3)P, phosphatidylinositol 3-phosphate; $PI(3,4)P_2$, phosphatidylinositol 3,4-bisphosphate; $PI(4,5)P_2$, phosphatidylinositol 4,5-bisphosphate; $PI(3,4,5)P_3$, phosphatidylinositol 3,4,5-trisphosphate; TRIF, TIR-domain-containing adaptor protein inducing IFNβ; TRAM, TRIF-related adaptor molecule; MAL, MyD88-adaptor-like; OCRL, oculocerebrorenal syndrome of Lowe; PLC, phospholipase C.

the release of IFNβ and IL-10 (9). Rab8a is initially recruited to the membranes of dorsal ruffles on the macrophage cell surface, where the TLR4-Mal-MyD88 complex is also located (9). Dorsal ruffles collapse to form macropinosomes or contribute to the formation of phagosomes for the uptake of fluid phase solutes or pathogens and particles, respectively (10–12). TLR4 in ruffles is poised for incorporation into membranes of endosomal compartments, where a change in the signaling adaptors to TRAM and TRIF facilitates the distinct switch in signaling and gene expression outputs (7).

Given the spatial and temporal coupling between cell surface dorsal ruffles and endocytic pathways and the distribution of signaling sites for TLR family members across these membrane domains, here we explored the potential for Rab8a to recruit PI3Kγ for regulation of additional TLR pathways. Traditionally, the leukocyte-specific PI3Kγ has been viewed as a regulator downstream of receptor tyrosine kinase (RTK) and G protein-coupled receptor pathways, where its most prominent role is in chemotactic recruitment of cells to sites of inflammation (13, 14). Pharmacologic inhibition of PI3Kγ is considered a possible avenue for new therapeutics in cancer and inflammatory diseases (15, 16). PI3Kγ function downstream of TLRs/IL-1 receptors (IL-1Rs) (16) and TLR4 (9, 15) expands the regulatory sphere of this kinase beyond cellular recruitment, to the signals that actually initiate inflammation. Exploring other members of the TLR family will thus demonstrate the spectrum of exogenous pathogen-derived and endogenous host-derived danger signals that induce PI3Kγ-mediated signaling. Here we examine the role of the Rab8a-PI3Kγ axis in skewing macrophage inflammatory responses downstream of multiple TLRs.

Results

Rab8a Activation by TLR Agonists—We previously showed that Rab8a recruits PI3Kγ for Akt/mTOR signaling downstream of LPS-activated TLR4 (9). TLR3 and 9 signal as endosomal receptors (4), and here we compared the ability of TLR3, 4, and 9 agonists to activate Rab8a (Fig. 1). A GST fusion protein comprised of the Rab binding domain from the $PI(4,5)P_2$ 5-phosphatase OCRL, another Rab8 effector protein (17), was used for pulldowns of the active, GTP-bound Rab8a from macrophage extracts. The assay was calibrated using extracts preloaded with exogenous GDP or GTP at different concentrations (Fig. 1, *A* and *B*). Pulldowns from cells treated with TLR agonists for 0, 2, 10, and 60 min show rapid activation of Rab8a (Fig. 1*C*). Both LPS/TLR4 and poly(I:C)/TLR3 result in an ~2.5-fold increase in active Rab8a 10 min post-stimulation, whereas the TLR9 agonist CpG DNA (CpG) caused a more modest but sustained activation of Rab8a over 60 min. Thus, multiple TLR agonists activate Rab8a. In its active, GTP-bound form, Rab8a should recruit effectors, and indeed, GFP-Rab8a immunoprecipitates its effector PI3Kγ in response to all three TLR agonists (Fig. 1*D*). These results reveal that activation of Rab8a downstream of TLR4, 3, or 9 results in recruitment of PI3Kγ, suggesting a broader role for this GTPase-PI3K complex in diverse TLR pathways.

Rab8a Is Localized to TLR Signaling Domains on Ruffles and Macropinosomes—We showed previously that Rab8a is initially enriched on membranes of dorsal ruffles at the cell surface (9) and now show in live cells that these domains are sites where the dorsal ruffles close over into circular macropinosomes (Fig. 2*A*). These are confirmed to be genuine macropinosomes because they are found loaded with dextran and are not detected by post-fixation wheat germ agglutinin (WGA), which does not access fully closed macropinosomes (Fig. 2*B*). Hence, although Rab8a is initially in ruffle membranes, it is then found enriched in macropinosomes.

Co-expression of Rab8a with other endosomal markers shows that GFP-Rab8a does not overlap with mCherry-Rab5a on small punctate early endosomes in live cells, whereas time-lapse analysis of macropinosomes reveals the conversion of the membrane from Rab8a-enriched to Rab5a as the macropinosome matures (Fig. 2*C*). Finally, tdTomato-Rab8a was coexpressed with markers that cycle between recycling endosomes and the plasma membrane, namely transferrin (Tfn-647) and GFP-VAMP3 (Fig. 2*D*). In triple-labeled, fixed cells, there is significant overlap between VAMP3 and Tfn but little overlap with Rab8a. This is further highlighted on line scans showing that Rab8a peak fluorescence is at the plasma membrane and macropinosomes (Fig. 2*D*, *i*) while being offset from recycling endosome markers (Fig. 2*D*, *ii*). We can thus conclude that, in macrophages, Rab8a is most prominent on dorsal ruffle membranes and early macropinosomes.

The conversion of dorsal ruffles to macropinosomes is also accompanied by a transition in phosphoinositides from plasma membrane $PI(4,5)P_2$, which is converted to $PI(3,4,5)P_3$ and $PI(3,4)P_2$ (11, 18). This spatiotemporal control of phosphoinositides can influence TLR signaling in two ways: the TLR adaptor Mal dissociates from membranes (and TLRs) when $PI(4,5)P_2$ is depleted from endocytic membranes (7), and enhanced $PI(3,4,5)P_3$ is the first step in the activation of the Akt/mTOR pathway (19). This transition can be tracked in live cells with plasmid-encoded fluorescent phosphoinositide probes such as PH-PLCδ-GFP, which recognizes $PI(4,5)P_2$, and the PH domain from Akt, which recognizes both $PI(3,4,5)P_3$ and $PI(3,4)P_2$ (Fig. 3, *A* and *B*). Coexpressed Rab8a is first present on $PI(4,5)P_2$-containing ruffles that close over into circular macropinosomes that then lose $PI(4,5)P_2$ during scission from the plasma membrane (Fig. 3*A*). Rab8a is retained on membranes as they acquire $PI(3,4,5)P_3$, peaking in intensity alongside Akt-PH-GFP in early macropinosomes (Fig. 3*B*). Finally, Rab8a labeling dissociates as the membranes accumulate early endosome-associated PI(3)P, which is recognized by 2xFYVE-mCherry on more mature macropinosomes (Fig. 3*C*), and Rab5a, which is responsible for the production of PI(3)P (Fig. 2*C*). These results are consistent with the enrichment of Rab8a in newly forming signaling macropinosomes. Live-cell imaging of full-length GFP-Akt additionally designates these early dorsal ruffles and macropinosomes as the site of Akt recruitment to macropinosomes (supplemental Fig. S2). The results obtained with the Akt-PH probe (Fig. 3*B*) and full-length proteins (supplemental Fig. S2) thus indicate that Rab8a is enriched at signaling domains along with $PI(3,4,5)P_3$ and Akt.

Rab8a and Akt enrichment in early macropinosomes is relevant to this compartment as a locale for TLR-driven PI3K signaling. Accordingly, Rab8a colocalizes both with Mal on ruffles and newly forming macropinosomes in addition to the TLR

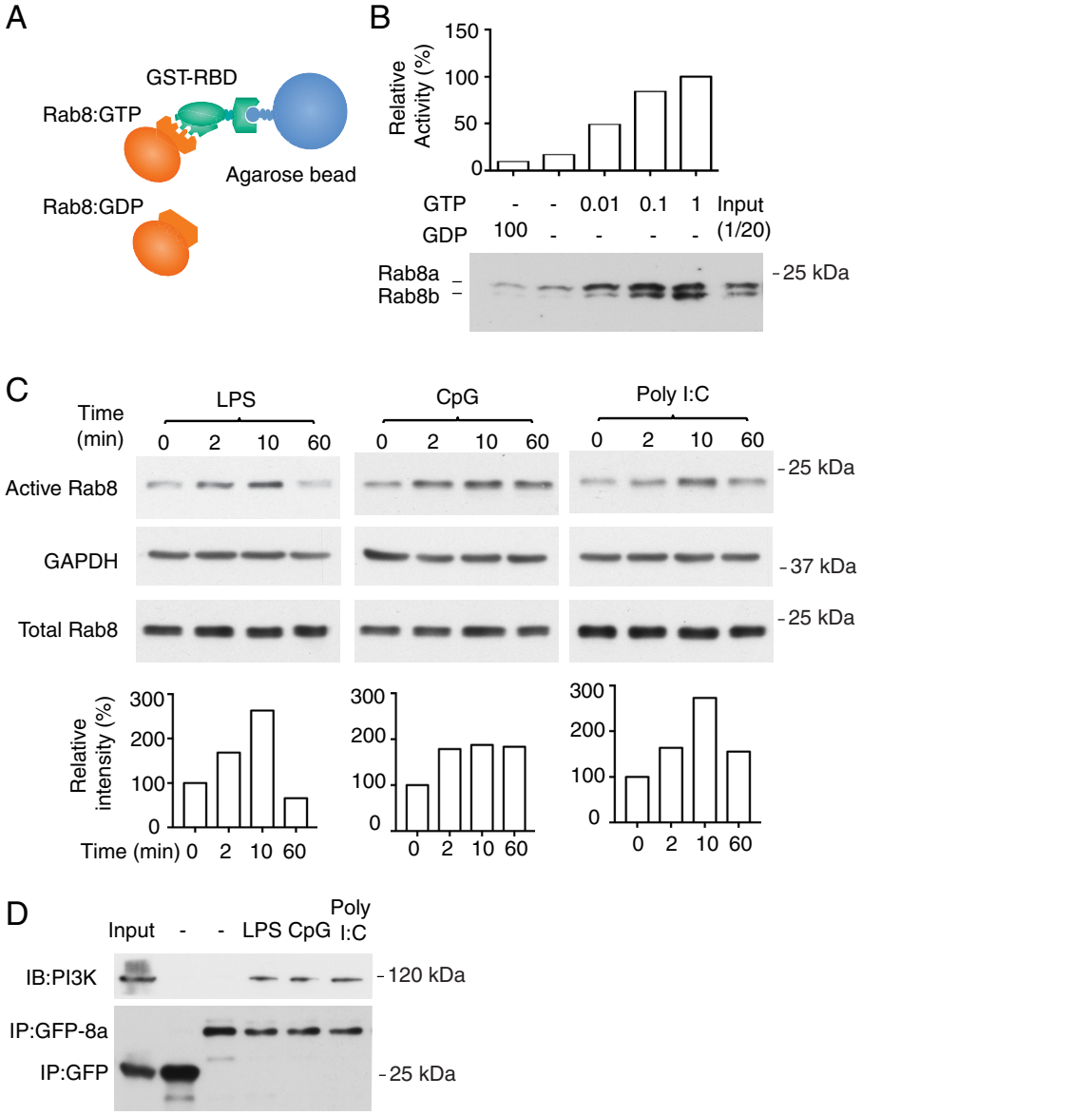

FIGURE 1. **Activated Rab8 recruits class IB PI3Kγ in response to multiple TLR stimuli.** *A*, schematic of the Rab8 activation assay. GST-OCRL-RBD, via its RBD, specifically pulls down GTP-loaded Rab8. *B*, immunoblots of active Rab8 (GTP-Rab8) with various levels of GTP in RAW 264.7 macrophages. *C*, immunoblots of active Rab8 (GTP-Rab8) in LPS, poly(I:C), CpG-activated RAW 264.7 macrophages. The level of Rab8 activation is quantified based on the ratio of active Rab8 relative to total Rab8 by using densitometry. *D*, GFP-Rab8a was stably expressed in RAW264.7 macrophages. Cells were treated with LPS, CpG, or poly(I:C) or not treated, and the GFP antibody was used for immunoprecipitation (*IP*). Each experiment (*B–D*) was performed three times, and the gels are representative. *IB*, immunoblot.

adaptor for endosomal signaling, TRAM (Fig. 3, *D* and *E*). Therefore, Rab8a is on membranes that are positioned to support signaling from TLRs 4, 3, and 9, which act at both the cell surface and/or only in endosomes (20).

Rab8a Modulates TLR Signaling from Macropinosomes—To further explore roles for Rab8a in TLR signaling, we developed CRISPR/Cas9-mediated Rab8a knockout cell lines from RAW 264.7 cells. Instead of isolation and expansion of clonal populations with insertion or deletion (INDEL) mutations, we used homologous recombination to disrupt the first intron of *Rab8a* using a neomycin expression cassette (supplemental Fig. S1). This is of particular importance in maintaining a large heterogeneous population of cells in the RAW 264.7 cell line. After selection, Rab8a protein expression was undetectable in KO cells, whereas expression of Rab8b was unaffected (supplemental Fig. S1*D*).

Using these Rab8a CRISPR KO cell lines, Akt phosphorylation was assessed over a time course in cells treated with LPS, CpG, or poly(I:C) (Fig. 4*A*). Representative gels and densitometry analysis revealed that, at early time points, there is a >50% decrease in the phosphorylation of Akt in response to all three agonists compared with controls. This early defect in Akt phosphorylation is recovered at later time points in Rab8a KO cells. The decrease in p-Akt levels was the major pathway affected by Rab8a depletion compared with the more subtle decrease in phosphorylation of Erk1/2 observed after activation of TLR4, 3, and 9 (Fig. 4*A* and supplemental Fig. S3*A*). Thus, loss of Rab8a impairs TLR4, 3, and 9-mediated activation of Akt.

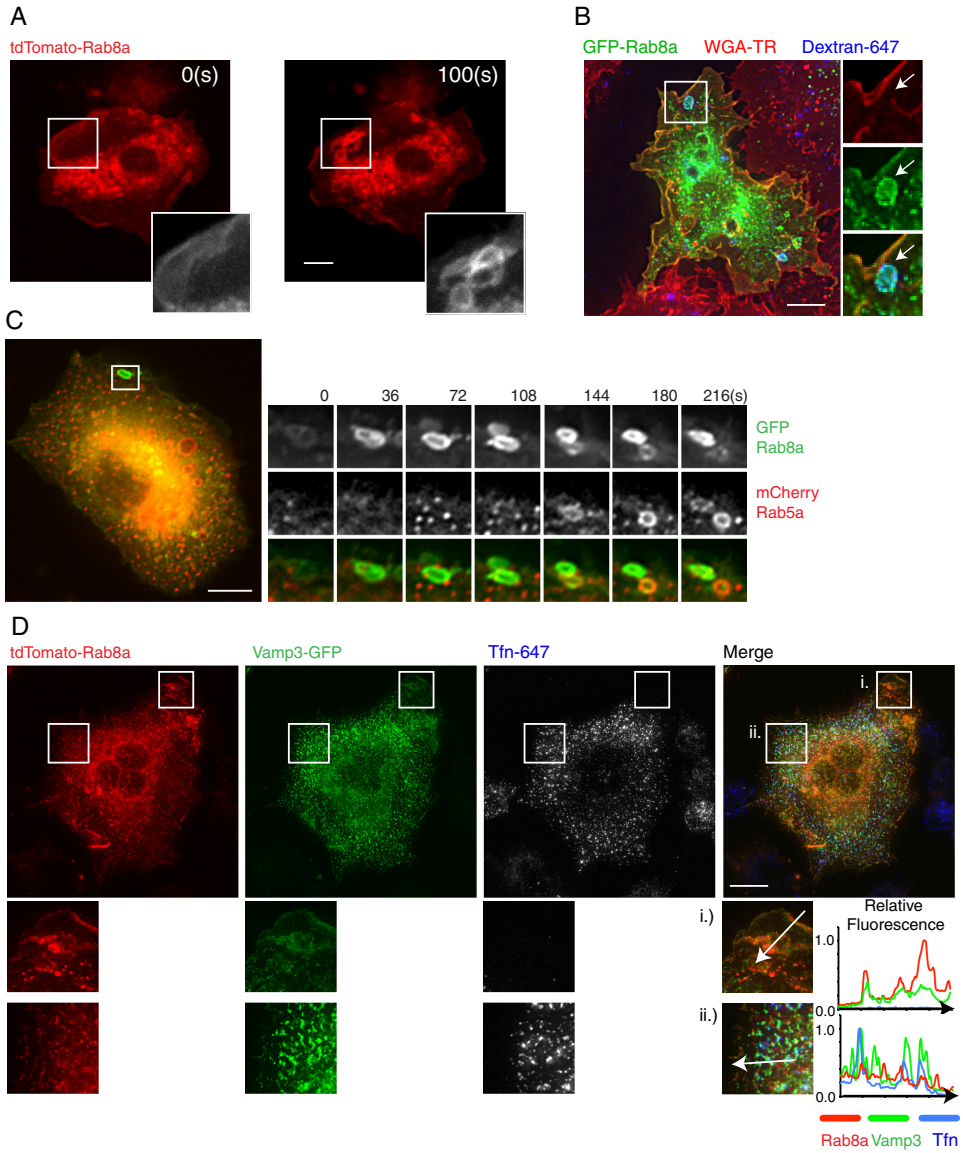

FIGURE 2. **Rab8a is localized to TLR signaling domains on ruffles and macropinosomes.** *A*, live-cell imaging of RAW 264.7 macrophages transiently transfected with td-Tomato-Rab8a and treated with 100 ng/ml LPS. *Left panel*, the presence of Rab8a on peripheral ruffles. *Right panel*, the collapsed ruffle enriched in Rab8-positive macropinosome-like structures. *B*, RAW 264.7 macrophages transfected with GFP-Rab8a were pulsed with Alexa 647 dextran for 10 min. Fixed cells were co-labeled with Texas Red-WGA to label the cell surface. GFP-Rab8a can be found co-localized with dextran-positive macropinosomes. *C*, live-cell imaging of cells transfected with GFP-Rab8a and mCherry-Rab5a. Cells were treated with 100 ng/ml LPS and imaged over a time course. Tracking shows a Rab8a-enriched macropinosome converting to Rab5a as Rab8a is lost. *D*, RAW 264.7 macrophages transfected with tdTomato-Rab8a and Vamp3-GFP were loaded with Tfn-647 for 10 min and chased for 10 min at 37 degrees. *i*, line scan (direction of arrow) analysis of surface ruffle and macropinosome. *ii*, line scan analysis of recycling endosomes. *Scale bars* = 10 μm.

To address the possibility of off-target effects, Rab8a recovery cell lines were generated by stably expressing exogenous V5-tagged Rab8a to restore Rab8a expression in the CRISPR/Cas9 Rab8a KO cells to almost wild-type levels (supplemental Fig. S3*B*, *exo-Rab8*). As matched controls, V5-empty vector was used in both control and KO cells. Re-expression of Rab8a in all cases restored TLR-inducible Akt activation (Fig. 4*B*), further supporting the conclusion that Rab8a positively regulates Akt signaling downstream of TLR4, 3, and 9.

The Effector PI3Kγ Is Required for TLR-induced Akt/mTOR Signaling and Regulation of Cytokine Responses—Having shown previously that PI3Kγ is the Rab8a effector that modulates Akt/mTOR signaling in response to LPS/TLR4 (9), we next used BMMs from p110γ catalytic subunit knock-out mice (PI3K$\gamma^{-/-}$) to compare TLR-mediated signaling events. Phospho-Akt levels are markedly decreased in PI3K$\gamma^{-/-}$ BMMs after challenge with LPS, as identified previously (9). Representative densitometry analysis of Akt phosphorylation in macrophages stimulated with poly(I:C) or CpG reveal that this response is reduced at early time points (Fig. 5, *A* and *B*), reflecting the result obtained after depletion of Rab8a. The downstream influence of this delay in Akt phosphorylation in PI3K$\gamma^{-/-}$ BMMs was assessed by phosphorylation analysis of the Akt substrate PRAS40, mTOR, and one of its substrates, p70S6K. Overall, delayed or reduced Akt phosphorylation results in reduced levels of PRAS40 across all TLR pathways (Fig. 5*A*). Other responses show some divergence between TLR pathways. Phosphorylation of mTOR and its substrate p70S6K

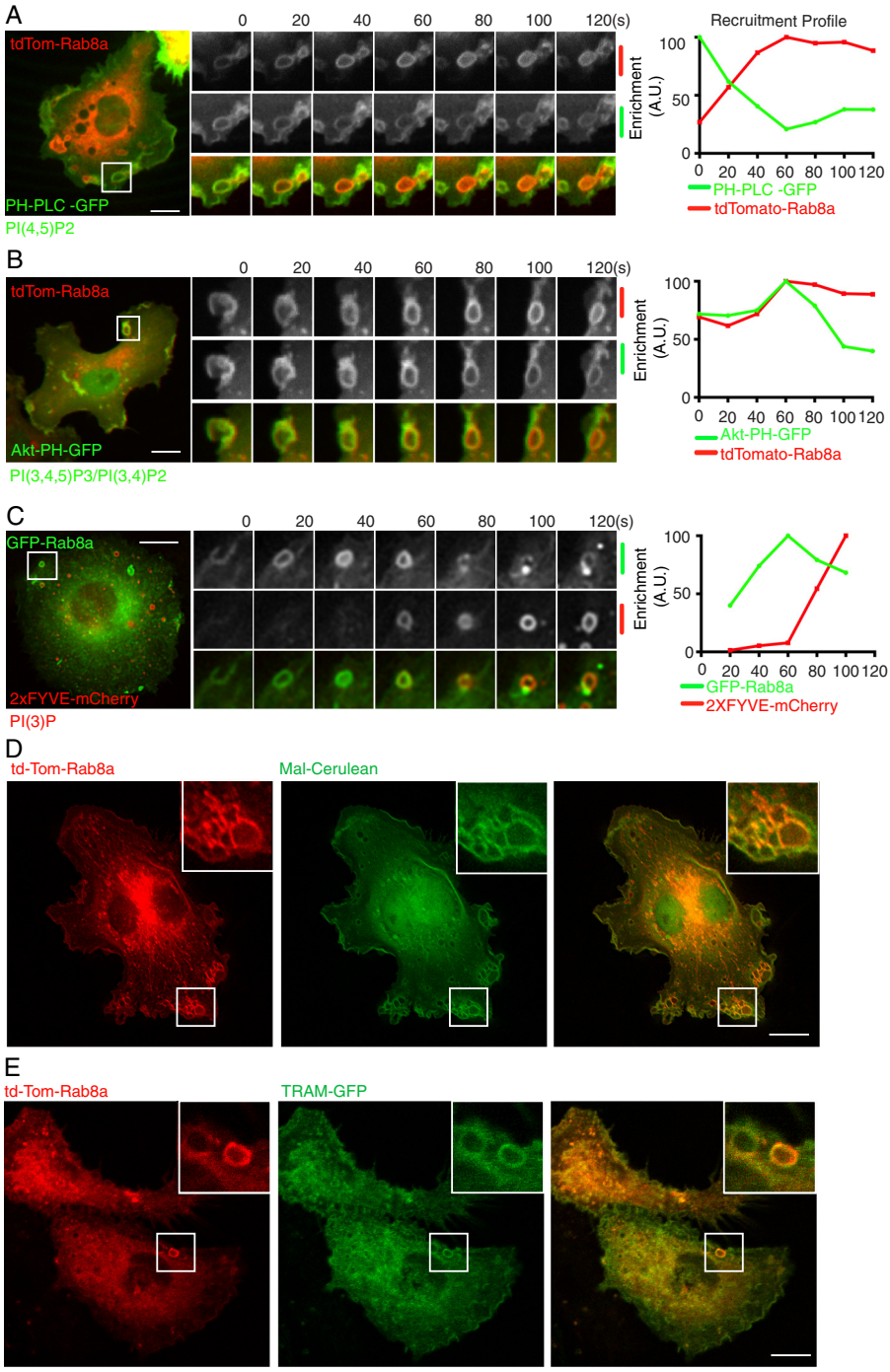

FIGURE 3. **Rab8a colocalizes with PI(3,4,5)P during macropinosome formation.** *A* and *B*, live-cell imaging of RAW 264.7 cells co-expressing full-length tdTomato-Rab8a, and PH-PLCδ-GFP (*A*) or Akt-PH-GFP (*B*) was used to assess the enrichment of $PI(4,5)P_2$ or $PI(3,4,5)P_3$ in Rab8a-positive macropinosomes. *C*, RAW264.7 cells cotransfected with full-length GFP-Rab8a and 2xFYVE-mCherry were used to examine the enrichment of PI(3)P in Rab8a-positive macropinosomes. *D*, image of RAW264.7 macrophages transfected with Mal-Cerulean and tdTomato-Rab8a showing the co-localization at macropinosomes. E, image of RAW264.7 macrophages transfected with TRAM-GFP and tdTomato-Rab8a showing the co-localization at macropinosomes. Arbitrary unit (*A.U.*) = percentage of maximum fluorescence intensity. *Scale bars* = 10 μm.

are decreased after LPS and poly(I:C) stimulation but not in CpG-stimulated cells. Interestingly, this is reflected in decreased phosphorylation of the CREB transcription factor by LPS and poly(I:C), which is indirectly downstream of p70S6K (21). PI3K$\gamma^{-/-}$ BMMs showed only a very modest enhancement of LPS-induced p65 phosphorylation at 15 min post-stimulation, suggesting that NF-κB activation is not a major target of this kinase downstream of TLR engagement. Finally, in PI3K$\gamma^{-/-}$ BMMs, there is a modest increase in TLR-inducible Erk1/2 phosphorylation compared with wild-type cells (Fig. 5*A* and supplemental Fig. S4*A*). Based on these results, we conclude that Rab8a-recruited PI3Kγ contributes to Akt signaling downstream of not only TLR4 but also of TLR3 and 9. Moreover, this signaling module appears to be particularly important for mTOR activation downstream of TLR4 and 3 in comparison with TLR9.

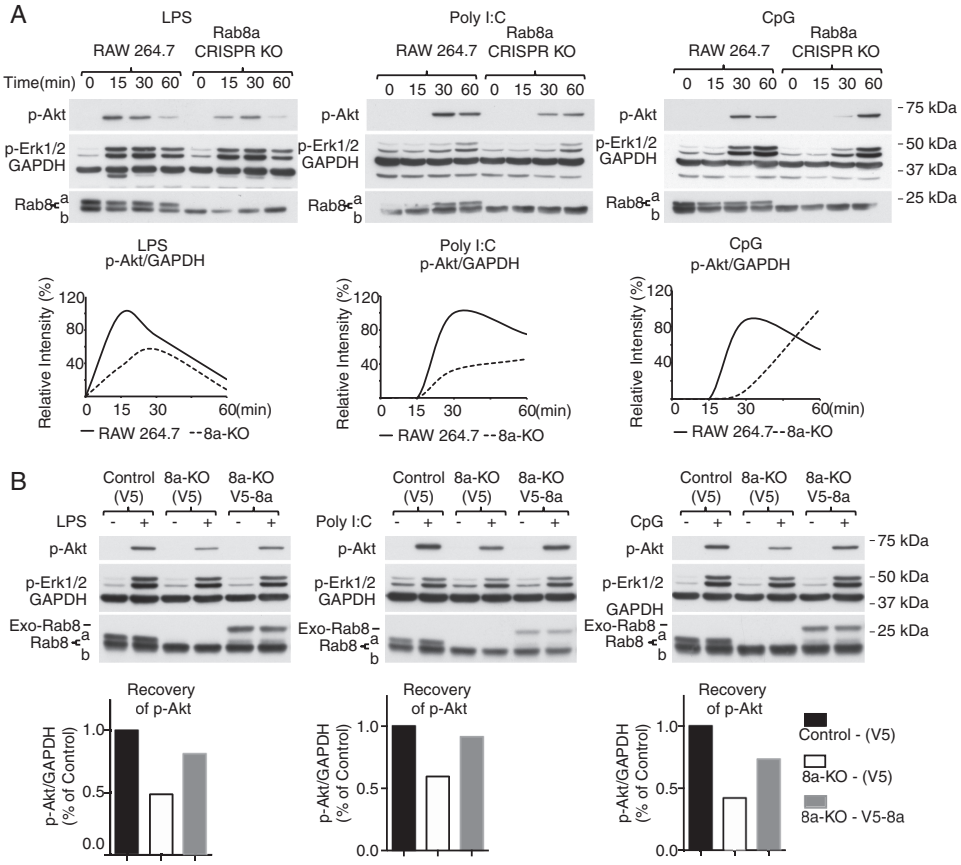

FIGURE 4. **Rab8a regulation of endosomal TLRs.** *A*, representative immunoblot analysis of the LPS, poly(I:C), and CpG time courses for control and CRISPR-mediated Rab8a knockout RAW 264.7 cell lines. Cell extracts were analyzed for Akt, Erk1/2 phosphorylation, and GAPDH. Phosphorylation of Akt and GAPDH was analyzed 0, 15, 30, or 60 min post-TLR stimulation by densitometry, and the gels are representative of three independent experiments. *B*, representative immunoblot analysis of 15-min LPS, 30-min poly(I:C), and CpG post-TLR stimulation for control, CRISPR-mediated Rab8a knockout, and V5-tagged Rab8a rescue-expressed recovery RAW 264.7 cell lines. Phosphorylation of Akt and GAPDH was analyzed by densitometry, and the gels are representative of three independent experiments ($n = 3$ each).

We reported previously that loss of PI3Kγ impaired neither LPS-induced macropinocytosis nor the internalization of TLR4 itself (9). Here we show that Rab8a-deficient and PI3Kγ$^{-/-}$ macrophages exhibit comparable levels of dextran loading compared with control cells (supplemental Fig. S5). Therefore, although Rab8a and PI3Kγ are recruited to membranes undergoing macropinocytosis, they do not influence this process *per se* but, rather, contribute specifically to enhancing the signaling environment of the membrane subdomains, which results in enhanced phosphorylation of Akt from macropinosomes.

TLR signaling directs transcriptional programs of inflammatory and regulatory cytokines. In PI3Kγ$^{-/-}$ BMMs, LPS stimulation results in increased secretion of proinflammatory IL-6 and IL-12p40 and reduced secretion of the regulatory cytokine IL-10 (Fig. 5*C*). CpG stimulation revealed similar patterns for the proinflammatory response; however, there are no differences in IL-10 secretion between PI3Kγ$^{-/-}$ and WT macrophages (Fig. 5*C*). In contrast, in response to poly(I:C) stimulation, IL-12p40 secretion was similar in PI3Kγ$^{-/-}$ and WT macrophages, whereas IL-10 secretion was markedly reduced (Fig. 5*C*). IL-6 secretion in response to poly(I:C) was not detectable under these experimental conditions. Thus, altered signaling in PI3Kγ$^{-/-}$ cells changes cytokine outputs from the endosomal TLRs but with variable effects on the inflammatory response. Therefore, Rab8a-recruited PI3Kγ is required for Akt/mTOR signaling and inflammatory cytokine responses generated by both plasma membrane-initiated TLR4 as well as endosomal TLR3 and 9. This highlights the early macropinosome and the associated Rab8a-PI3Kγ complex as major functional components that dictate the cytokine program initiated during TLR activation.

PI3Kγ Attenuates TLR-driven Proinflammatory Cytokine Responses in Human Macrophages—As PI3Ks are known to have both enzymatic and scaffolding functions *in vivo* (22), we inhibited the function of PI3Kγ using the γ-selective inhibitor AS605240. As this inhibitor is only 7.5-fold more selective for PI3Kγ than PI3Kα, we performed a titration of AS605240 in BMMs derived from PI3Kγ$^{-/-}$ mice that were stimulated with CSF-1. The results from the AS605240 titration experiment show that the optimal concentration for the inhibitor is 1 μM, whereas, at higher concentrations of 10 and 20 μM, the inhibitor showed significant off-target effects (supplemental Fig. S4*B*). Next, we examined the phosphorylation of Akt in response to LPS and CpG in both mouse macrophages and in human monocyte-derived macrophages (HMDMs) (Fig. 6, *A–D*). In keeping with the effects of genetic ablation of PI3Kγ, pharmacologic inhibition decreases the phosphorylation of Akt in response to LPS and CpG in both mouse and human cells. This supports an active

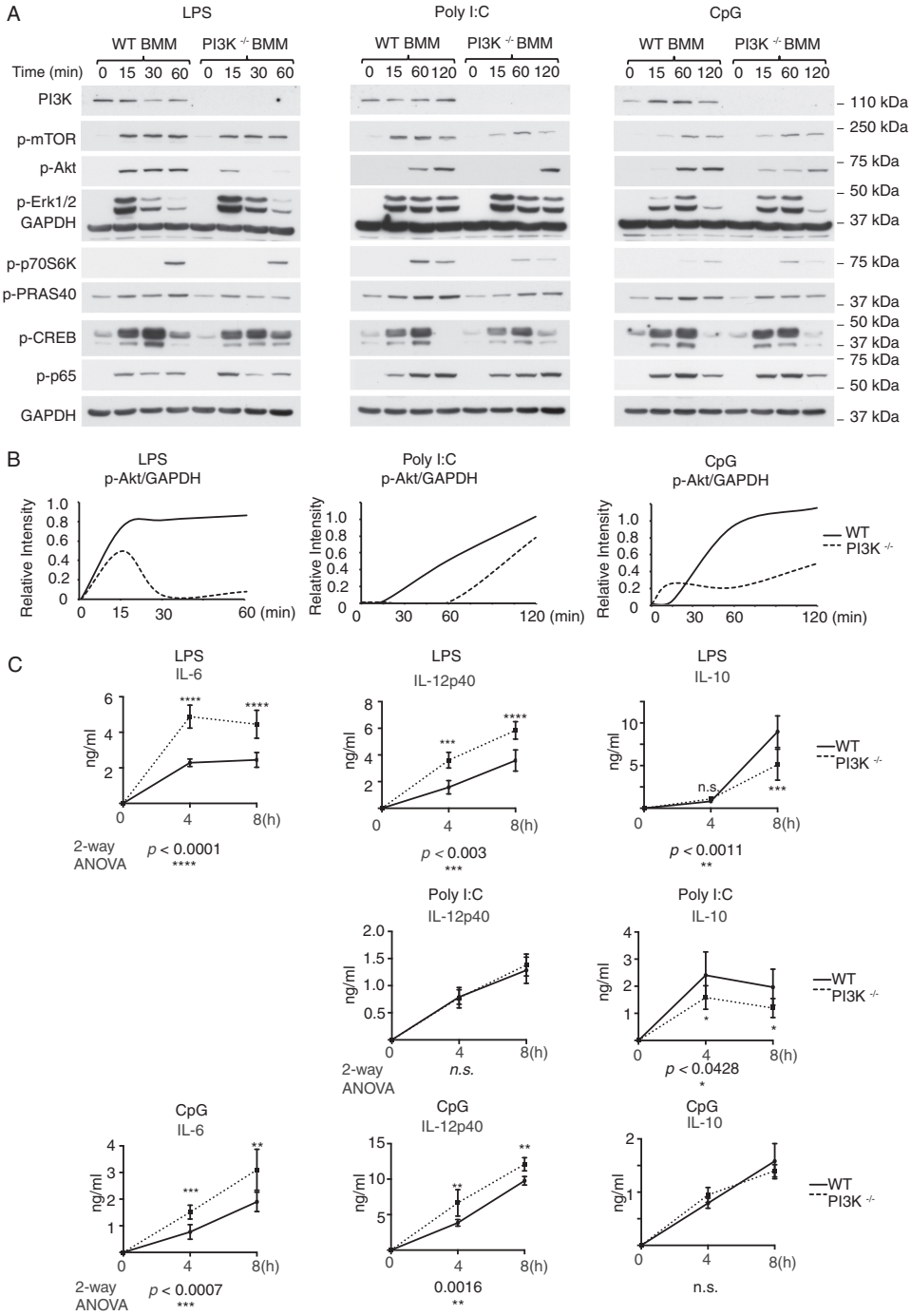

FIGURE 5. **PI3Kγ regulates TLR-mediated endosomal signaling and cytokines in macrophages.** *A*, BMMs derived from WT and PI3K$\gamma^{-/-}$ animals were subjected to a 60-min time course of LPS or a 120-min time course of poly(I:C) and CpG. Cell extracts were analyzed for PI3Kγ, Akt, Erk1/2, mTOR, p70S6K, PRAS40, CREB, and p65 phosphorylation and GAPDH. *B*, quantification of the phosphorylation of Akt and total GAPDH was performed by densitometry analysis. The graphs indicate representative quantification of p-Akt relative to GAPDH for each time course. *C*, cytokine concentrations in medium were measured by ELISA after LPS, poly(I:C), or CpG treatment. Each data point is the mean ± S.D. ($n = 5$). Statistical analyses were performed using two-way ANOVA with Sidak's post-test for multiple comparisons (*, $p < 0.05$; **, $p < 0.01$; ***, $p < 0.001$; ****, $p < 0.0001$).

kinase function for PI3Kγ in modulating Akt signaling in macropinosomes during TLR-induced activation of macrophages.

We also examined the downstream cytokine responses to LPS in human cells using both primary HMDMs (Fig. 6) and a human cell line (supplemental Fig. S4*C*) to monitor regulated gene expression. Inhibition of PI3Kγ with AS605240 results in a significant increase in mRNA expression of the proinflammatory cytokines IL-6 and IL-12p40 in response to LPS compared with cells treated with DMSO (Fig. 6*E*). In contrast, mRNA levels of IL-10 are significantly suppressed in AS605240-treated cells at every time point analyzed. This supports our previous findings in mouse macrophages, thus demonstrating that PI3Kγ inhibition works equivalently in murine and human macrophages to affect the acute inflammatory response.

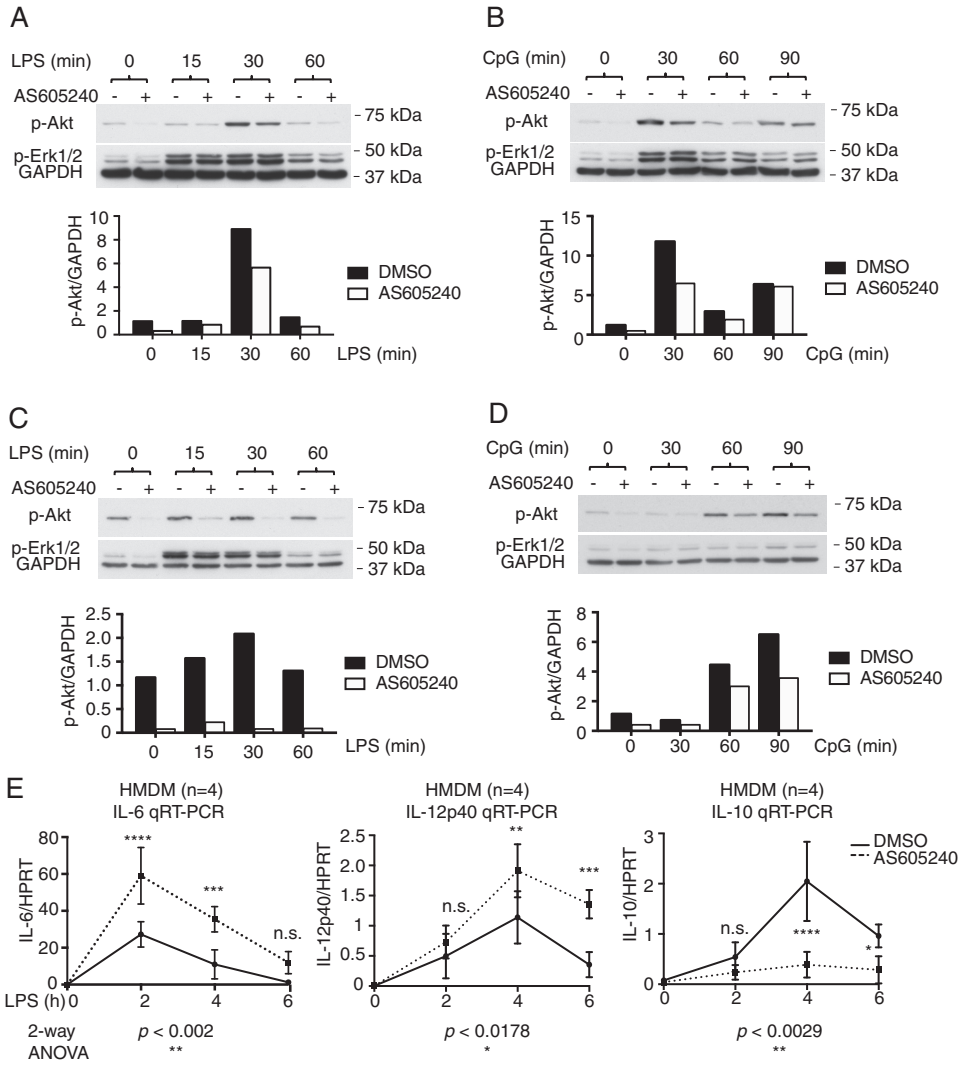

FIGURE 6. **Pharmacological inhibition of PI3Kγ and TLR responses in both human and mouse macrophages.** *A* and *B*, RAW 264.7 cells were treated with either vehicle (DMSO) or 1 μM AS605240 for 30 min before addition of (*A*) LPS or (*B*) CpG over a 60- or 90-min time course, respectively. Cell extracts were analyzed for phosphorylation of Akt and Erk1/2 compared with GAPDH as a control. *C* and *D*, HMDMs were treated with either vehicle (DMSO) or 1 μM of AS605240 for 30 min before addition of (*C*) LPS or (*D*) CpG over a 60- or 90-min time course, respectively. Cell extracts were analyzed for phosphorylation of Akt and Erk1/2 compared with GAPDH as a control. Quantification of representative ($n = 3$ each) p-Akt levels for each blot is shown. *E*, transcriptional responses were analyzed by quantitative RT-PCR in both control (DMSO) or AS605240-treated HMDMs subjected to a 6-h LPS time course. Graphs represent mean ± S.D. ($n = 4$ each). Profiles were analyzed by two-way ANOVA, and the significance of individual time points was measured by Sidak post-test for multiple comparisons.

Discussion

Signaling pathways downstream of activated TLRs in macrophages are necessarily complex to elicit responses to a range of pathogens. This includes triggering varied transcriptional programs that shape the profile of secreted inflammatory cytokines. We previously introduced the multifunctional GTPase Rab8a, with PI3Kγ as its effector, as a signaling platform that regulates Akt/mTOR activation downstream of LPS-activated TLR4 to constrain inflammatory responses (9). Here, by exploring additional pathogen-associated molecular patterns (PAMPs) and their cognate TLR receptors, we reveal that Rab8a-PI3Kγ also serves to moderate downstream Akt signaling and cytokine profiles for TLR3 and 9. Notably, this includes regulation of signaling and cytokine responses elicited from endosomal locales. Our data pinpoint the site of action for Rab8a recruited PI3Kγ to early macropinosomes. Mechanistically, our findings suggest that PI3Kγ contributes to formation of $PI(3,4,5)P_3$ for attraction of signaling kinases, including Akt, in macropinosomes for the modulation of cytokine output.

The Rab8a localization we show in activated macrophages is commensurate with its presence on membranes at cell surfaces, at leading edges and on membrane vesicles, and from the surface (23, 24). Within this distribution, we show a specific and dramatic recruitment of Rab8a first to dorsal ruffles on the surface of LPS-activated macrophages, along with adaptors of the surface TLR4 complex. Rab8a remains on these highly dynamic dorsal ruffle membranes as they collapse and form macropinosomes, where Rab8a is enriched along with the signaling phosphoinositide $PI(3,4,5)P_3$. It should be noted that additional PI3K isoforms are recruited for macropinosome closure (11), and neither loss of PI3Kγ (Ref. 9 and supplemental Fig. S5) nor Rab8a (supplemental Fig. S5) affects macropinocytosis itself.

Therefore, Rab8a recruits its effector PI3Kγ to signaling-competent membranes that transition between the cell surface and macropinosome.

The molecular mechanism of PI3K activation by TLRs and their adaptors is poorly understood. So far, only class 1A PI3Ks have been described in this context. A pioneering study by Arbibe *et al.* (25) suggested that Y*XX*M motifs in TLRs are necessary for the recruitment of class IA PI3K, via the p85 regulatory subunit, to the signaling complex. Another study suggests that the TLR signaling adapter MAL links TLR2 signaling to PI3K activation (26). We showed previously that, although TLR4 results in the activation of Rab8a and the recruitment of PI3Kγ, neither this GTPase nor the kinase bind directly to the TLR4 complex (9). As an independent unit, Rab8a and its class IB effector, PI3Kγ, are potentially available to be recruited by other receptors. Mechanistically, this explains how Rab8a-PI3Kγ, as an independent regulatory unit, is available to be recruited for multiple TLR pathways where this complex functions to modulate or customize Akt signaling. Ultimately, the method for recruiting PI3Kγ to membranes via a Rab GTPase instead of its traditional Ras partner and the Gβγ subunit of an activated G protein-coupled receptor complex (13) will have to be elucidated.

TLR signaling pathways use complex series of kinases and substrates to drive transcription of pro- and anti-inflammatory cytokines (27). Rab8a and PI3K depletion show consistent changes in activation of Akt and its substrate across all three TLR pathways examined. This and previous studies (9, 28) show that the LPS/TLR4 pathway drives an Akt/mTOR axis that can bias cytokines toward a less inflammatory profile. Our comparison of three TLR pathways here reveals that mTOR signaling is activated by LPS and poly(I:C) but not significantly by CpG. Accordingly, activation of CREB (21, 29) in the TLR4 and 3 pathways might contribute to the anti-inflammatory cytokine output influenced by PI3Kγ, but additional transcriptional control must be invoked in the TLR9 response. Detailed links between PI3Kγ-mediated signaling and transcription, downstream of TLRs, have yet to be elucidated.

TLR signaling also depends on the selective use of different adaptor combinations by different TLRs. Rab8a and PI3Kγ are downstream of TLR4, which transits between cell surface (ruffle) complexes with MyD88-MAL to an endosomal complex with TRIF-TRAM. Rab8a and PI3Kγ are also invoked by endosomal complexes of TLR3 (TRIF-TRAM-dependent) and TLR9 (MyD88-dependent). We show that Rab8a is on membranes, where it overlaps with Mal (on surface ruffles), and in macropinosomes, where it overlaps with TRAM. The patterns of cytokine responses altered by Rab8a-PI3Kγ suggest that this regulatory complex can influence the cytokine profile elicited from both sets of adaptors. There are some differences in the impact on specific cytokines, and the molecular mechanisms underlying these remain to be determined. Our data in Fig. 5*C* support a model in which PI3Kγ negatively regulates IL-6 and Il-12p40 in MyD88-dependent signaling (LPS, CpG), whereas it positively regulates IL-10 in the TRIF pathway (LPS, poly(I:C)). Both the localization and functional outputs of Rab8a-PI3Kγ are consistent with this complex being downstream of both MyD88-Mal and TRIF-TRAM adaptors on the surface and in macropinosomes.

PI3Kγ has attracted interest as a potential drug target in cancer and other diseases (15, 30). PI3Kγ-specific inhibitors are currently undergoing clinical trials in patients with advanced solid tumors, including non-small cell lung cancer and melanoma (31). Kaneda *et al.* (15) recently showed that inhibition of PI3Kγ reprograms macrophages and enhances anti-tumor immune responses by releasing pro-inflammatory cytokines that activate cytotoxic T cells. However, in the context of bacterial and viral infections, our results suggest that PI3Kγ inhibition bears the risk of hyperinflammatory responses. Further studies are needed to dissect the role of PI3Kγ and the clinical consequences of inhibitory targeting of PI3Kγ during infections.

Experimental Procedures

Antibodies and Reagents—Primary antibodies recognizing PI3Kγ (4252), phospho-mTOR (5536), phospho p65 (3033), phospho-CREB (9198), phospho-PRAS40 (2997), phospho-p70 S6 kinase (Thr-389, 9234), phospho-Akt (Ser-473, 4962), phospho-Erk1/2 (4370), and GAPDH (5174) were purchased from Cell Signaling Technology (Beverly, MA). Mouse anti-Rab8 (610845) was purchased from BD Transduction Laboratories (Lexington, KY). Anti-GFP antibody (A6455) was purchased from Life Tech Australia (Scoresby, VIC, Australia). GST antibody (71-7500) was purchased from Invitrogen. Alexa Fluor 488/594-conjugated (A21208) and 647-conjugated (A31573) secondary antibodies, 10,000 molecular weight Alexa Fluor 647-dextran 70,000 molecular weight Oregon Green-dextran, and Texas Red-WGA were purchased from Molecular Probes (Invitrogen). HRP-conjugated goat anti-mouse and anti-rabbit antibodies (81-6520) were obtained from Zymed Laboratories Inc. (San Francisco, CA). LPS, purified from *Salmonella enterica* serotype Minnesota Re 595, was purchased from Sigma-Aldrich (Castle Hill, NSW, Australia). The CpG-containing oligonucleotide ODN-1688 (5′-tccatgacgttcctgatgct-3′, where all nucleotides are phosphorothioate-modified) was purchased from Genscript. The synthetic double-stranded RNA poly(I:C) was purchased from Integrated Sciences (Chatswood, NSW, Australia). LPS, poly(I:C), and CpG DNA were used at 10–100 ng/ml, 10 μg/ml, and 0.3 μM, respectively, unless otherwise stated. AS605240 was purchased from Sigma-Aldrich. All other chemicals and reagents were from Sigma-Aldrich. Gibson Assembly® Master Mix was from New England Biolabs (E2611, Ipswich, MA). The GeneArt® genomic cleavage detection kit (A24372) was from Invitrogen (Thermo Fisher Scientific).

Plasmid and Constructs—Rab8a was subcloned into pEGFP-C1, pm-Cherry-C1, and ptd-Tomato-C1, which had been generated from pCMV-tdTomato (Clontech, Clayton, VIC, Australia). Constructs containing Akt-PH-GFP, PH-PLCδ-GFP, and 2xFYVE-mCherry were kindly provided by Frederic Meunier (University of Queensland). Mal-Cerulean was a gift from Nicholas J. Gay (University of Cambridge). Full-length TRAM was cloned from RAW 264.7 cDNA into the Clontech vector pEGFP-N1 using the BamHI and HindIII restriction sites and the following primers: forward, 5′-AATTGGATCC CGGGCAATGAACTGTTTCTG-3′; reverse, 5′-AATTAAG-CTTATGGGTGTTGGGAAGTCT-3′. pSpCas9n(BB)-2A-GFP

(PX461) was from Feng Zhang (Addgene plasmid 48140). Human OCRL (residues 539–901) was cloned into pGEX-6p-1.

Rab8 Activation Assay—The Rab8 activation assay utilizes a GST fusion protein of the Ras-binding domain (RBD) of OCRL (amino acids 539–901) along with glutathione-Sepharose resin to specifically pull down active GTP-loaded Rab8 detected with an anti-Rab8 antibody for Western blotting. Briefly, cells were lysed in lysis buffer (20 mM Tris (pH 7.4), 150 mM NaCl, 1% Nonidet P-40 (Sigma), 5 mM $MgCl_2$, and EDTA-free cOmplete protease inhibitors (Roche Applied Science)). GST-OCRL-RBD-Sepharose beads were incubated with cell lysate for 1 h at 4 °C with agitation. MicroSpin columns (27-3565-01, GE Healthcare) were used for all of the pulldowns. Beads were washed with ice-cold lysis buffer (above), and elution was achieved conventionally by boiling in 2× SDS-PAGE sample buffer for 5 min. The samples were subjected to immunoblots.

Immunoprecipitation and Immunoblot—Immunoprecipitation and immunoblots were performed as described previously (32). Briefly, cells were lysed by passage through successively smaller needles in lysis buffer (above), which also contained phospho-Stop tablets (Roche Applied Science). After centrifugation at 14,000 × *g* for 15 min, the supernatant was collected and used as input. For immunoprecipitations, cell lysates were incubated with GFP Nanotrap for 1 h at 4 °C. Beads were then washed with excess lysis buffer, and bound proteins were solubilized in SDS-PAGE sample buffer. Proteins were separated by 10% SDS-PAGE and analyzed by immunoblotting. For time course analysis, Pierce BCA protein assay kits (23225) were used to quantify total protein in cell lysates according to the instructions of the manufacturer.

Generation of Rab8a CRISPR/Cas9-mediated KO in RAW 264.7 Macrophages—The first exon of *Rab8a*, which contains the translation start site and downstream coding sequence, was chosen to design two parallel CRISPRs that would "nick" the 5′ and 3′ strand to generate a specific double-stranded break (supplemental Fig. S1*A*). Primer pairs were cloned into the px461 vector developed by Feng Zhang (33): px461-1, 5′-CACCGCAGCTTGAACAGGTAATCGT-3′ (forward) and 5′-AAACACGATTACCTGTTCAAGCTGC-3′ (reverse); px461-2 5′-CACCGTGATCGGG GACTCGGGGGTA-3′ (forward) and 5′-AAACTACCCC CGAGTCCCCGATCAC-3′ (reverse). For cleavage analysis, RAW 264.7 macrophages were transfected using the Lonza AMAXA nucleofection system (nucleofector kit V-VCA-1003) and the D032 program. Cells were transfected with the following modification from the instructions of the manufacturer. For each nucleofection, 5×10^6 cells were transfected with either 2.5 μg of individual px461–1 or px461–2 plasmids as controls or co-transfected with both plasmids. Each transfection contained 2 μg of empty neomycin plasmid, and cells were selected for 3 days before being harvested for cleavage analysis with the GeneArt® genomic cleavage detection kit, which utilizes two primers (supplemental Fig. S1*B*, *red*) flanking the CRISPR cut site (forward, 5′-AGATGTGACCACACCCATCG-3′; reverse, 5′-ACAAAGCACCCATCACGAGT-3′) that are predicted to generate an 877-bp amplicon (Fig. 1*C*). For generation of the Rab8a donor vector for gene disruption, two genomic arms flanking the left and right CRISPR cut sites were cloned from RAW 264.7 genomic DNA. A nearly 2-kb left homology arm was PCR-amplified using 5′-TCGAGATTTAATTAAGA TACGCGTGACGATTTTGGGCCAGAGAGAGCACGAGG-3′ (forward) and 5′-GAATAGGAACTTCGGTAAAGCTTATCCGATGCGAAAGCGGCGCAGAG (reverse). The 1.4-kb right homology arm was PCR-amplified using 5′-CGGTATATATATATATATGTCGACATGGTTATCGACTCAGGATCCACTCGGGC-3′ (forward) and 5′-AGATCTGCGATCGCAATCAATTGCTGGTTACCCTCTGCTTCCTCCAGACTGA-3′ (reverse). Each primer contained 30 bp of extended sequence, which allows for GIBSON assembly of the donor vector that overlaps with the neomycin selection plasmid containing diphtheria toxin A as a negative selection cassette for random integration events (supplemental Fig. S1*C*). To generate stable cell lines with disruption of Rab8a, px461-1 and px461-2 were co-transfected along with the donor vector for homologous recombination. 24 h post-transfection, cells were selected with 0.1 μg/μl G418 for 5 days for mixed colony expansion and testing for Rab8a KO by Western blotting (supplemental Fig. S1*D*).

Ethics Statement—All procedures involving animals were approved by an Animal Ethics Committee of The University of Queensland (approval no. IMB/026/15/NHMRC/ARC (NF)). All experiments using primary human cells were approved by the Medical Research Ethics Committee of the University of Queensland (approval no. 2013001519).

Primary Cells and Cell Lines—The mouse macrophage cell line RAW 264.7 was sourced from the ATCC. RAW 264.7 macrophages were cultured in RPMI 1640 medium (Lonza) supplemented with 10% heat-inactivated FCS (Thermo Fisher Scientific) and 2 mM L-glutamine (Invitrogen) at 37 °C in humidified 5% CO_2. THP-1 cells were maintained in RPMI 1640 supplemented medium with added 1 mM sodium pyruvate and 10 mM HEPES. THP-1 cells were differentiated into macrophage-like cells by culture for 72 h in normal THP-1 medium containing 30 ng/ml phorbol 12-myristate 13-acetate (Sigma Aldrich). After differentiation, cells were replaced in normal medium without phorbol 12-myristate 13-acetate and used thereafter. Mice deficient in the p110γ catalytic subunit (pik3cg2/2, PI3K$\gamma^{-/-}$) have been described previously (34). Age-matched (12–16 weeks) and sex-matched C57BL/6 mice were used as controls. Primary mouse bone marrow-derived macrophages (BMMs) were obtained by *ex vivo* differentiation of femur-derived bone marrow cells for 7 days in RPMI medium supplemented with 10% fetal bovine serum, 20 units/ml penicillin, 20 μg/ml streptomycin, and 100 ng/ml purified recombinant macrophage colony-stimulating factor 1 (CSF-1) (35, 36). HMDMs were prepared from $CD14^+$ monocytes isolated from buffy coats supplied by the Australian Red Cross Blood Service. Monocytes were differentiated into HMDMs by culturing cells with 1×10^4 units/ml CSF-1 for 6 days as described previously (37).

Immunofluorescence and Microscopy—Immunofluorescence staining was performed as described previously (38). For live-cell experiments, RAW 264.7 macrophages were cultured on glass-bottom 35-mm dishes (MatTek). Live-cell imaging was captured using the Zeiss spinning disk confocal system (Zeiss Axiovert 200 with a CSU-X1 scanhead), a Plan Apochromatic ×60/1.40 oil lens, and dual 512 × 512 cameras. Fixed cells were

imaged using a Personal DeltaVision Olympus IX71 inverted wide-field deconvolution microscope equipped with Olympus U-Apochromat ×40/1.35 oil and a Plan-Apochromat ×60/1.42 oil lens and a 120-W xenon arc lamp. Images were captured using a Roper Coolsnap HQ2 monochrome camera.

Dextran Uptake Assays—RAW 264.7 macrophages were incubated with or without LPS for 30 min. Oregon Green-conjugated dextran (70,000 molecular weight) was then added to the cells at a final concentration of 50 μg/ml in complete medium for 10 min. Macropinocytosis was stopped by washing cells in 4 °C PBS before fixing in 4% paraformaldehyde. Texas Red-WGA and DAPI were used post-fixation to stain the cell surface and nuclei, respectively. Cells were imaged using an Olympus BX51 upright microscope and a Plan Apochromatic 20 × 0.75 dry objective.

Enzyme-linked Immunosorbent Assays and Quantitative Real-Time PCR—ELISAs were performed to quantify levels of IL-6, IL-12p40, and IL-10 secreted from BMMs. 96-well Maxisorp plates (Thermo Scientific) were coated with 50 μl of primary antibody in 0.1 M sodium bicarbonate at pH 9.6 overnight at 4 °C. Plates were then washed with PBST (PBS/0.05% Tween 20), blocked with 200 μl of blocking buffer (10% FCS in PBS) for 2 h at 37 °C, and then incubated with 100 μl of standards or samples overnight at 4 °C. Plates were again washed with PBST, treated with 50 μl of secondary antibody made up in blocking buffer for 1 h at 37 °C, and washed with PBST. 100 μl of extravidin-peroxidase (1:1000) was added, and then samples were incubated for 20–30 min at 37 °C. Peroxidase activity was measured colorimetrically by adding 50 μl of tetramethylbenzidine substrate (Sigma-Aldrich), and the reaction was stopped by addition of 50 μl of 2 M H_2SO_4. The absorbance was read at 450 nm using a Powerwave XS plate reader, and the sample concentrations were calculated. Quantitative RT-PCR was performed as described previously (9). Briefly, RNA was extracted and isolated using TRIzol® (Thermo Fisher Scientific, Australia), as per the manufacturer's instructions. cDNA was synthesized by reverse transcription using 1 g of total RNA per sample using the SuperScript™ III First-Strand Synthesis System (Invitrogen). All primers used are listed as follows: HPRT 5′-TCAGGCAGTATAATCCAAAGATGGT-3′ (forward) and 5′-AGTCTGGCTTATATCCAACACTTCG-3′ (reverse); IL-6 5′-CTCAGCCCTGAGAAAGGAGACAT-3′ (forward) and 5′-TCAGCCATCTTTGGAAGGTTCA-3′ (reverse); IL-12p40 5′-GGAGACCATCAAGGAAGACATGA-3′ (forward) and 5′-GACTCCCGTGCAGTCATCC-3′ (reverse); and IL-10 5′-CGAAGGCCAACATCAATGTGG-3′ (forward) and 5′-TCCGGTGTGATTTTGACTCCC-3′ (reverse).

Image Analysis Software—Imaging analyses of all data were performed using ImageJ software (version 1.43, National Institutes of Health). Adobe Photoshop CS6 was used to crop regions of interest.

Statistics—Unless otherwise stated, data are presented as arithmetic means ± S.D. For quantitative RT-PCR, time courses were analyzed by two-way ANOVA, and individual time points were analyzed by correcting for multiple comparisons using Sidak's post-test method. All analyzed experiments used biological replicates to compute statistical significance. In all statistical analyses, $p < 0.05$ was considered statistically significant. Statistics were calculated using GraphPad Prism version 7.0 (GraphPad Software, San Diego, CA).

Author Contributions—A. A. W., L. L., and J. L. S. conceived the project, designed the experiments, analyzed the data, and wrote the manuscript. Y. H. conducted the experiments and analysis shown in Fig. 6 and supplemental Fig. S4. N. D. C. performed the experiments and data collection for supplemental Fig. S5. S. J. T. collected the data for Fig. 5*A*. A. B. and M. J. S. contributed to design and data interpretation and manuscript preparation. All experiments using human cells were performed in the laboratory of M. J. S.

Acknowledgments—We thank Juliana Venturato and Tatiana Khromykh for expert technical assistance, colleagues as acknowledged for reagents, and the Australian Red Cross Blood Service for providing buffy coats, which were used for the isolation of human monocytes. We thank Claudia Stocks and Ronan Kapetanovic for assistance with culturing human monocytes. Imaging was performed in the Australian Cancer Research Foundation-funded Cancer Biology Imaging Facility at IMB.

References

1. O'Neill, L. A., and Bowie, A. G. (2007) The family of five: TIR-domain-containing adaptors in Toll-like receptor signalling. *Nat. Rev. Immunol.* **7,** 353–364
2. Stow, J. L., and Murray, R. Z. (2013) Intracellular trafficking and secretion of inflammatory cytokines. *Cytokine Growth Factor Rev.* **24,** 227–239
3. Leifer, C. A., and Medvedev, A. E. (2016) Molecular mechanisms of regulation of Toll-like receptor signaling. *J. Leukocyte Biol.* **100,** 927–941
4. Rossol, M., Heine, H., Meusch, U., Quandt, D., Klein, C., Sweet, M. J., and Hauschildt, S. (2011) LPS-induced cytokine production in human monocytes and macrophages. *Crit. Rev. Immunol.* **31,** 379–446
5. Vercammen, E., Staal, J., and Beyaert, R. (2008) Sensing of viral infection and activation of innate immunity by Toll-like receptor 3. *Clin. Microbiol. Rev.* **21,** 13–25
6. Bonham, K. S., Orzalli, M. H., Hayashi, K., Wolf, A. I., Glanemann, C., Weninger, W., Iwasaki, A., Knipe, D. M., and Kagan, J. C. (2014) A promiscuous lipid-binding protein diversifies the subcellular sites of Toll-like receptor signal transduction. *Cell* **156,** 705–716
7. Kagan, J. C., and Medzhitov, R. (2006) Phosphoinositide-mediated adaptor recruitment controls Toll-like receptor signaling. *Cell* **125,** 943–955
8. Cohen, H. B., and Mosser, D. M. (2013) Extrinsic and intrinsic control of macrophage inflammatory responses. *J. Leukocyte Biol.* **94,** 913–919
9. Luo, L., Wall, A. A., Yeo, J. C., Condon, N. D., Norwood, S. J., Schoenwaelder, S., Chen, K. W., Jackson, S., Jenkins, B. J., Hartland, E. L., Schroder, K., Collins, B. M., Sweet, M. J., and Stow, J. L. (2014) Rab8a interacts directly with PI3Kγ to modulate TLR4-driven PI3K and mTOR signalling. *Nat. Commun.* **5,** 4407
10. Patel, P. C., and Harrison, R. E. (2008) Membrane ruffles capture C3bi-opsonized particles in activated macrophages. *Mol. Biol. Cell* **19,** 4628–4639
11. Welliver, T. P., and Swanson, J. A. (2012) A growth factor signaling cascade confined to circular ruffles in macrophages. *Biol. Open* **1,** 754–760
12. Yeo, J. C., Wall, A. A., Luo, L., and Stow, J. L. (2015) Rab31 and APPL2 enhance FcγR-mediated phagocytosis through PI3K/Akt signaling in macrophages. *Mol. Biol. Cell* **26,** 952–965
13. Vadas, O., Dbouk, H. A., Shymanets, A., Perisic, O., Burke, J. E., Abi Saab, W. F., Khalil, B. D., Harteneck, C., Bresnick, A. R., Nürnberg, B., Backer, J. M., and Williams, R. L. (2013) Molecular determinants of PI3Kγ-mediated activation downstream of G-protein-coupled receptors (GPCRs). *Proc. Natl. Acad. Sci. U.S.A.* **110,** 18862–18867
14. Regad, T. (2015) Targeting RTK signaling pathways in cancer. *Cancers* **7,** 1758–1784
15. Kaneda, M. M., Messer, K. S., Ralainirina, N., Li, H., Leem, C. J., Gorjestani, S., Woo, G., Nguyen, A. V., Figueiredo, C. C., Foubert, P., Schmid, M. C., Pink, M., Winkler, D. G., Rausch, M., Palombella, V. J., *et al.* (2016) PI3Kγ

is a molecular switch that controls immune suppression. *Nature* **539,** 437–442
16. Schmid, M. C., Avraamides, C. J., Dippold, H. C., Franco, I., Foubert, P., Ellies, L. G., Acevedo, L. M., Manglicmot, J. R., Song, X., Wrasidlo, W., Blair, S. L., Ginsberg, M. H., Cheresh, D. A., Hirsch, E., Field, S. J., and Varner, J. A. (2011) Receptor tyrosine kinases and TLR/IL1 Rs unexpectedly activate myeloid cell PI3Kγ, a single convergent point promoting tumor inflammation and progression. *Cancer Cell* **19,** 715–727
17. Hagemann, N., Hou, X., Goody, R. S., Itzen, A., and Erdmann, K. S. (2012) Crystal structure of the Rab binding domain of OCRL1 in complex with Rab8 and functional implications of the OCRL1/Rab8 module for Lowe syndrome. *Small GTPases* **3,** 107–110
18. Yoshida, S., Hoppe, A. D., Araki, N., and Swanson, J. A. (2009) Sequential signaling in plasma-membrane domains during macropinosome formation in macrophages. *J. Cell Sci.* **122,** 3250–3261
19. Vanhaesebroeck, B., Stephens, L., and Hawkins, P. (2012) PI3K signalling: the path to discovery and understanding. *Nat. Rev. Mol. Cell Biol.* **13,** 195–203
20. Barton, G. M., and Kagan, J. C. (2009) A cell biological view of Toll-like receptor function: regulation through compartmentalization. *Nat. Rev. Immunol.* **9,** 535–542
21. Turnquist, H. R., Cardinal, J., Macedo, C., Rosborough, B. R., Sumpter, T. L., Geller, D. A., Metes, D., and Thomson, A. W. (2010) mTOR and GSK-3 shape the CD4+ T-cell stimulatory and differentiation capacity of myeloid DCs after exposure to LPS. *Blood* **115,** 4758–4769
22. Damilano, F., Perino, A., and Hirsch, E. (2010) PI3K kinase and scaffold functions in heart. *Ann. N.Y. Acad. Sci.* **1188,** 39–45
23. Hattula, K., Furuhjelm, J., Tikkanen, J., Tanhuanpää, K., Laakkonen, P., and Peränen, J. (2006) Characterization of the Rab8-specific membrane traffic route linked to protrusion formation. *J. Cell Sci.* **119,** 4866–4877
24. Peränen, J. (2011) Rab8 GTPase as a regulator of cell shape. *Cytoskeleton* **68,** 527–539
25. Arbibe, L., Mira, J. P., Teusch, N., Kline, L., Guha, M., Mackman, N., Godowski, P. J., Ulevitch, R. J., and Knaus, U. G. (2000) Toll-like receptor 2-mediated NF-κ B activation requires a Rac1-dependent pathway. *Nat. Immunol.* **1,** 533–540
26. Santos-Sierra, S., Deshmukh, S. D., Kalnitski, J., Küenzi, P., Wymann, M. P., Golenbock, D. T., and Henneke, P. (2009) Mal connects TLR2 to PI3Kinase activation and phagocyte polarization. *EMBO J.* **28,** 2018–2027
27. Dunne, A., and O'Neill, L. A. (2003) The interleukin-1 receptor/Toll-like receptor superfamily: signal transduction during inflammation and host defense. *Sci STKE* **2003,** re3
28. Ivanov, S. S., and Roy, C. R. (2013) Pathogen signatures activate a ubiquitination pathway that modulates the function of the metabolic checkpoint kinase mTOR. *Nat. Immunol.* **14,** 1219–1228
29. Coudriet, G. M., He, J., Trucco, M., Mars, W. M., and Piganelli, J. D. (2010) Hepatocyte growth factor modulates interleukin-6 production in bone marrow derived macrophages: implications for inflammatory mediated diseases. *PLoS ONE* **5,** e15384
30. Rückle, T., Schwarz, M. K., and Rommel, C. (2006) PI3K γ inhibition: towards an "aspirin of the 21st century"? *Nat. Rev. Drug. Discov.* **5,** 903–918
31. Evans, C. A., Liu, T., Lescarbeau, A., Nair, S. J., Grenier, L., Pradeilles, J. A., Glenadel, Q., Tibbitts, T., Rowley, A. M., DiNitto, J. P., Brophy, E. E., O'Hearn, E. L., Ali, J. A., Winkler, D. G., Goldstein, S. I., *et al.* (2016) Discovery of a selective phosphoinositide-3-kinase (PI3K)-γ inhibitor (IPI-549) as an immuno-oncology clinical candidate. *ACS Med. Chem. Lett.* **7,** 862–867
32. Luo, L., Xue, J., Kwan, A., Gamsjaeger, R., Wielens, J., von Kleist, L., Cubeddu, L., Guo, Z., Stow, J. L., Parker, M. W., Mackay, J. P., and Robinson, P. J. (2016) The binding of syndapin SH3 Domain to dynamin proline-rich domain involves short and long distance elements. *J. Biol. Chem.* **291,** 9411–9424
33. Ran, F. A., Hsu, P. D., Wright, J., Agarwala, V., Scott, D. A., and Zhang, F. (2013) Genome engineering using the CRISPR-Cas9 system. *Nat. Protoc.* **8,** 2281–2308
34. Hirsch, E., Katanaev, V. L., Garlanda, C., Azzolino, O., Pirola, L., Silengo, L., Sozzani, S., Mantovani, A., Altruda, F., and Wymann, M. P. (2000) Central role for G protein-coupled phosphoinositide 3-kinase γ in inflammation. *Science* **287,** 1049–1053
35. Hume, D. A., and Gordon, S. (1982) Regulation of bone-marrow macrophage proliferation. *Adv. Exp. Med. Biol.* **155,** 261–266
36. Tushinski, R. J., Oliver, I. T., Guilbert, L. J., Tynan, P. W., Warner, J. R., and Stanley, E. R. (1982) Survival of mononuclear phagocytes depends on a lineage-specific growth-factor that the differentiated cells selectively destroy. *Cell* **28,** 71–81
37. Ariffin, J. K., das Gupta, K., Kapetanovic, R., Iyer, A., Reid, R. C., Fairlie, D. P., and Sweet, M. J. (2015) Histone deacetylase inhibitors promote mitochondrial reactive oxygen species production and bacterial clearance by human macrophages. *Antimicrob. Agents Chemother.* **60,** 1521–1529
38. Murray, R. Z., Wylie, F. G., Khromykh, T., Hume, D. A., and Stow, J. L. (2005) Syntaxin 6 and Vti1b form a novel SNARE complex, which is up-regulated in activated macrophages to facilitate exocytosis of tumor necrosis factor-α. *J. Biol. Chem.* **280,** 10478–10483